AFRL-AFOSR-UK-TR-2010-0005

Magnesium Chemistry in the Upper Atmosphere

John M Plane
University of Leeds
School of Chemistry
Woodhouse Lane
Leeds, United Kingdom LS2 9JT

EOARD GRANT 09-3015

December 2010

Final Report for 11 December 2008 to 11 December 2010

Air Force Research Laboratory
Air Force Office of Scientific Research
European Office of Aerospace Research and Development
Unit 4515 Box 14, APO AE 09421

REPORT DOCUMENTATION PAGE

Form Approved OMB No. 0704-0188

1. REPORT DATE *(DD-MM-YYYY)*	2. REPORT TYPE	3. DATES COVERED *(From – To)*
21-12-2010	Final Report	11 December 2008 - 11 December 2010

4. TITLE AND SUBTITLE

Magnesium Chemistry in the Upper Atmosphere

5a. CONTRACT NUMBER
FA8655-09-1-3015

5b. GRANT NUMBER

5c. PROGRAM ELEMENT NUMBER

6. AUTHOR(S)

Professor John M Plane

5d. PROJECT NUMBER

5d. TASK NUMBER

5e. WORK UNIT NUMBER

7. PERFORMING ORGANIZATION NAME(S) AND ADDRESS(ES)

University of Leeds
Woodhouse Lane
Leeds LS2 9JT
United Kingdom

8. PERFORMING ORGANIZATION REPORT
Grant 09-3015

9. SPONSORING/MONITORING AGENCY NAME(S) AND ADDRESS(ES)

EOARD
Unit 4515 BOX 14
APO AE 09421

10. SPONSOR/MONITOR'S ACRONYM(S)

11. SPONSOR/MONITOR'S REPORT NUMBER(S)
AFRL-AFOSR-UK-TR-2010-0005

12. DISTRIBUTION/AVAILABILITY STATEMENT

Approved for public release; distribution is unlimited.

13. SUPPLEMENTARY NOTES

14. ABSTRACT

For this research the following objectives have been achieved:
- studied the reaction kinetics of Mg+ ions with O3, O2, N2, CO2, H2O and N2O using a laser flash photolysis-laser induced fluorescence technique
- studied the reactions of MgO+ and MgO2+ with atomic O, and a series of ligand-switching and association reactions of Mg+ cluster ions with O2, H2O and CO2, using a flow tube-mass spectrometry technique
- studied the reactions of MgO, MgO2, MgO3 and MgCO3 with atomic O using a flow tube- laser induced fluorescence technique
- produced a set of high-level quantum theory calculations of the thermochemistries of all these reactions
- completed an analysis of satellite observations (using the SCIAMACHY instrument on ENVISAT) of Mg and Mg+; this has shown that unlike other metals in the mesosphere, atomic Mg is not removed in the presence of noctilucent ice clouds
- developed a new model of magnesium chemistry in the mesosphere/lower thermosphere which predicts absolute densities of the Mg and Mg+ layers, including their seasonal variations, in excellent agreement with satellite observations.
- applied this model to determine the lifetimes of Mg+ ions in sporadic ion layers in the terrestrial and Martian atmospheres

15. SUBJECT TERMS
EOARD, Atmospheric Chemistry, Ionosphere

16. SECURITY CLASSIFICATION OF:			17. LIMITATION OF ABSTRACT	18, NUMBER OF PAGES	19a. NAME OF RESPONSIBLE PERSON
a. REPORT	b. ABSTRACT	c. THIS PAGE			Brad Thompson
UNCLAS	UNCLAS	UNCLAS	UL	22	19b. TELEPHONE NUMBER *(Include area code)* +44 (0)1895 616163

European Office of Aerospace Research and Development: award no. FA8655-09-1-3015

FINAL Report

Project Title: **Magnesium Chemistry in the Upper Atmosphere**

Start date: **1 January 2009** **Duration**: **24 months**

Organization: **University of Leeds**

Principal investigator: **Professor John M C Plane**
Contact details: School of Chemistry, University of Leeds
Leeds LS2 9JT, United Kingdom
Tel: (44) 113 3438044
Fax: (44) 113 3436401
Email: j.m.c.plane@leeds.ac.uk

Professor J. M. C. Plane
Principal Investigator

Date: 20th December 2010

Summary

The following objectives have been achieved:

- studied the reaction kinetics of Mg^+ ions with O_3, O_2, N_2, CO_2, H_2O and N_2O using a laser flash photolysis-laser induced fluorescence technique
- studied the reactions of MgO^+ and MgO_2^+ with atomic O, and a series of ligand-switching and association reactions of Mg^+ cluster ions with O_2, H_2O and CO_2, using a flow tube-mass spectrometry technique
- studied the reactions of MgO, MgO_2, MgO_3 and $MgCO_3$ with atomic O using a flow tube- laser induced fluorescence technique
- produced a set of high-level quantum theory calculations of the thermochemistries of all these reactions
- completed an analysis of satellite observations (using the SCIAMACHY instrument on ENVISAT) of Mg and Mg^+; this has shown that unlike other metals in the mesosphere, atomic Mg is *not* removed in the presence of noctilucent ice clouds
- developed a new model of magnesium chemistry in the mesosphere/lower thermosphere which predicts absolute densities of the Mg and Mg^+ layers, including their seasonal variations, in excellent agreement with satellite observations.
- applied this model to determine the lifetimes of Mg^+ ions in sporadic ion layers in the terrestrial and Martian atmospheres

Publications arising from the project:

Plowright, R. J., T. J. McDonnell, T. G. Wright, and J. M. C. Plane (2009), Theoretical Study of Mg^+-X and $[X\text{-}Mg\text{-}Y]^+$ complexes important in the chemistry of ionospheric magnesium (X, Y = H_2O, CO_2, N_2, O_2, and O), *Journal of Physical Chemistry*, *A 113*, 9354-9364.

Whalley, C. L., and J. M. C. Plane (2010), Meteoric ion layers in the Martian atmosphere, *Faraday Discussions, 147,* 349-368.

Martinez-Nunez, E., C. L. Whalley, D. Shalashilin, and J. M. C. Plane (2010), Dynamics of $Mg^+ + H_2O$ + He: Capture, Collisional Stabilization and Collision-Induced Dissociation, *Journal of Physical Chemistry A, 114, 6472-6479.*

Whalley, C.L., J. C. Gómez Martín, T. G. Wright and John M. C. Plane, A kinetic study of Mg^+ and Mg-containing ions reacting with O_3, O_2, N_2, CO_2, N_2O and H_2O: implications for magnesium ion chemistry in the upper atmosphere, under review at *Physical Chemistry Chemical Physics*.

Introduction

Metallic species are deposited into the Earth's upper atmosphere by the ablation of approximately 50 tonnes of interplanetary dust that enters the atmosphere each day.[1] The dust undergoes frictional heating to its melting point (~ 1800 K), after which metallic species ablate and are deposited in the mesosphere-lower thermosphere (MLT) region of the atmosphere (70 – 120 km).[2]

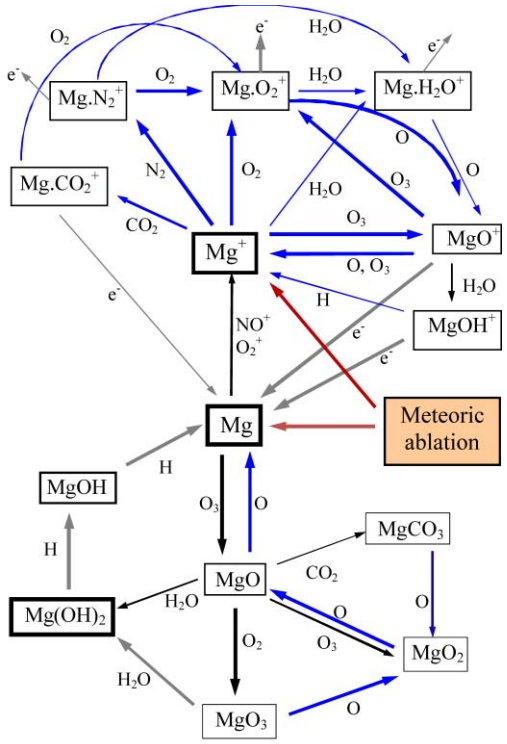

Figure 1. Schematic diagram of magnesium chemistry in the MLT. Blue arrows: reactions studied in the EOARD project. Black arrows: previously studied by the Leeds group. Grey arrows: remain to be studied, but rate constants can be estimated reliably. Thicker arrows indicate more important reaction pathways.

Magnesium is one of the most abundant metals in the MLT, with layers of Mg^+ being observed by rocket-borne mass spectrometry[3,4] and satellite observations of the earth's dayglow.[5-15] Recent satellite observations, made by the GOME[16] and SCIAMACHY[17,18] instruments, have found Mg to have a column density of ~ 2×10^9 cm^{-2}, with Mg^+ exhibiting column densities between 3×10^9 cm^{-2} at its winter minimum and 1.2×10^{10} cm^{-2} at its summer maximum at high latitudes. Mg^+ has a peak altitude between 90 and 100 km and a peak ion concentration of $(1 – 5) \times 10^3$ cm^{-3} during daylight, which declines to 10^2 cm^{-3} at night.[19] Mg exhibits lower concentrations and a peak altitude around 88 km.[17,20] Unlike the other prominent meteoric metals (Fe, Na, K and Ca), neither Mg nor Mg^+ can be observed by ground-based lidar (laser radar) as they have resonance transitions in the UV region at 285 and 280 nm respectively, where light is strongly absorbed by stratospheric O_3.

Mg^+ is produced from Mg by photo-ionization and charge transfer with NO^+ and O_2^+, which are the dominant ions in the lower thermosphere.[21] A striking difference between magnesium and other meteoric metals is the large ratio between Mg^+ and Mg. This ratio ranges from about 1.5 to more than 10. Magnesium seems to be the only metal displaying such a large ion/neutral ratio. Na^+/Na and Fe^+/Fe display ratios

of ~ 0.2[22,23] and Ca^+/Ca has a ratio of ~ 2.[24] This is even more striking as Mg^+ is not significantly depleted relative to other metals in the MLT.

Metallic ions, mainly Mg^+ and Fe^+,[22,25] are the major constituents of sporadic *E* layers (E_s). E_s are thin layers of concentrated plasma between 1 and 3 km wide, which occur at altitudes between 85 and 140 km.[26] They play an important role in over-the-horizon and space-to-ground radio communications.[27] Several mechanisms, including wind shear and gravity waves, have been proposed to explain their formation.[26]

Figure 1 is a schematic diagram of the chemistry of magnesium in the MLT. The blue arrows indicate the reactions studied in this EOARD project, demonstrating that the chemistry is now much better constrained and understood. Consider the ion-molecule chemistry first. Mg^+ ions are produced directly during meteoric ablation via hyperthermal collisions between Mg atoms and air molecules, and also by charge transfer between Mg and the ambient ions NO^+ and O_2^+ (solar photo-ionization of Mg is minor). Above 110 km the neutralization of Mg^+ by dielectric recombination ($Mg^+ + e^- \rightarrow Mg + h\upsilon$) is the only significant removal process of Mg^+ ions. However this process is very inefficient, with an estimated rate coefficient of 1×10^{-12} cm^3 s^{-1} [28] implying an average lifetime for Mg^+ in excess of 10 days.

At lower altitudes ion-molecule reactions become important:

$$Mg^+ + O_3 \rightarrow MgO^+ + O_2 \qquad \Delta H(0\ K) = -116\ kJ\ mol^{-1} \qquad (1)$$

$$Mg^+ + N_2 + M \rightarrow Mg^+.N_2 + M \qquad \Delta H(0\ K) = -30\ kJ\ mol^{-1} \qquad (2)$$

$$Mg^+ + O_2 + M \rightarrow MgO_2^+ + M \qquad \Delta H(0\ K) = -90\ kJ\ mol^{-1} \qquad (3)$$

$$Mg^+ + CO_2 + M \rightarrow Mg^+.CO_2 + M \qquad \Delta H(0\ K) = -67\ kJ\ mol^{-1} \qquad (4)$$

$$Mg^+ + H_2O + M \rightarrow Mg^+.H_2O + M \qquad \Delta H(0\ K) = -131\ kJ\ mol^{-1} \qquad (5)$$

where M is the third body (principally N_2 in the terrestrial atmosphere) which removes excess energy and stabilizes the association complex. The reaction enthalpy changes are determined from high-level quantum theory calculations which were published recently as part of this project.[29] Note that the molecular ion nomenclature adopted here is to indicate an ion where there is a chemical bond as MgX^+, and one where there is essentially only an electrostatic interaction as $Mg^+.X$.

Following the pioneering work at the NOAA Aeronomy Laboratory in the 1960s, formation of MgO^+ via reaction 1 is known to be rapid, and should dominate Mg^+ removal above 90 km in the terrestrial atmosphere.[30,31] Below 85 km, reaction with O_2 should become more important.[30] In contrast, reaction 4 dominates in the CO_2-rich Martian atmosphere.[32] Although the $Mg^+.N_2$ complex has been observed in the laboratory,[33] the kinetics of reaction 2 do not appear to have

been studied. Reaction 5 is comparatively fast,[34] but H_2O is a trace constituent and so this reaction should not be competitive.

The molecular ions formed by these reactions will eventually undergo very efficient dissociative recombination (DR) with an electron ($Mg^+.X + e- \rightarrow Mg + X$) to produce neutral Mg. However, before this occurs these ions can undergo rapid switching reactions, such as:

$$Mg^+.CO_2 + H_2O \rightarrow Mg^+.H_2O + CO_2 \qquad \Delta H(0\ K) = -64\ kJ\ mol^{-1} \qquad (6)$$

$$MgO_2^+ + H_2O \rightarrow Mg^+.H_2O + O_2 \qquad \Delta H(0\ K) = -41\ kJ\ mol^{-1} \qquad (7)$$

$$Mg^+.CO_2 + O_2 \rightarrow MgO_2^+ + CO_2 \qquad \Delta H(0\ K) = -23\ kJ\ mol^{-1} \qquad (8)$$

$$Mg^+.N_2 + O_2 \rightarrow MgO_2^+ + N_2 \qquad \Delta H(0\ K) = -60\ kJ\ mol^{-1} \qquad (9)$$

The Mg+.X cluster ions may also undergo addition reactions, in which a second ligand binds to the complex in the presence of a third body, M:

$$MgO_2^+ + O_2 \rightarrow MgO_2^+.O_2 \qquad \Delta H(0\ K) = -71\ kJ\ mol^{-1} \qquad (10)$$

$$Mg^+.CO_2 + CO_2 \rightarrow Mg^+.(CO_2)_2 \qquad \Delta H(0\ K) = -42\ kJ\ mol^{-1} \qquad (11)$$

$$Mg^+.H_2O + H_2O \rightarrow Mg^+.(H_2O)_2 \qquad \Delta H(0\ K) = -105\ kJ\ mol^{-1} \qquad (12)$$

$$MgO_2^+. + N_2 \rightarrow MgO_2^+.N_2 \qquad \Delta H(0\ K) = -96\ kJ\ mol^{-1} \qquad (13)$$

$$MgO_2^+ + CO_2 \rightarrow MgO_2^+.CO_2 \qquad \Delta H(0\ K) = -144\ kJ\ mol^{-1} \qquad (14)$$

$$Mg^+.H_2O + O_2 \rightarrow MgO_2^+.H_2O \qquad \Delta H(0\ K) = -173\ kJ\ mol^{-1} \qquad (15)$$

It has been suggested that formation of these larger cluster ions could be the first step in forming ice nuclei for noctilucent clouds in the mesosphere,[35] although this requires the clusters to grow very rapidly so that they are not completely destroyed when DR occurs.

Above 95 km, where the chemistry of E_s layers is of particular interest, MgO^+ formed in reaction 1 can react with O_3 via two exothermic channels:

$$MgO^+ + O_3 \rightarrow Mg^+ + 2O_2 \qquad \Delta H(0\ K) = -178\ kJ\ mol^{-1} \qquad (16a)$$

$$\rightarrow MgO_2^+ + O_2 \qquad \Delta H(0\ K) = -268\ kJ\ mol^{-1} \qquad (16b)$$

Atomic O is a major constituent of the lower thermosphere, and the sequence of reactions

$$MgO_2^+ + O \rightarrow MgO^+ + O_2 \qquad \Delta H(0\ K) = -126\ kJ\ mol^{-1} \qquad (17)$$

$$MgO^+ + O \rightarrow Mg^+ + O_2 \qquad \Delta H(0\ K) = -277\ kJ\ mol^{-1} \qquad (18)$$

reduces these oxide ions back to Mg^+. If reactions 17 and 18 compete effectively with DR, this will limit the efficiency with which Mg^+ is converted to Mg, thereby increasing the $[Mg^+]$ / [Mg] ratio and the lifetime of Mg^+ in an E_s layer.

It should be mentioned here that the reaction

$$MgO^+ + H_2O \rightarrow MgOH^+ + OH \qquad (19)$$

is fast.[31] However, above 80 km the ratio [O] / $[H_2O]$ is so large (>100) that reaction 19 is uncompetitive with reaction 17.

Reactions 1 and 3 have been studied previously at 300 K using the flowing afterglow technique, but the rate coefficients obtained were suggested to have an uncertainty exceeding a factor of 2.[30,31] Reactions 2 – 5 have been studied at 294 K using a selected-ion flow tube (SIFT) apparatus; however, in all cases no reaction was observed.[36] In this project reactions 1 - 18 were studied using the pulsed laser photolysis/laser induced fluorescence (PLP-LIF) and fast flow tube/mass spectrometer (FT-MS) techniques, where appropriate. We also studied the reaction

$$Mg^+ + N_2O \rightarrow MgO^+ + N_2 \qquad \Delta H(0\ K) = -55\ kJ\ mol^{-1} \qquad (20a)$$

$$\rightarrow Mg^+.N_2O \qquad \Delta H(0\ K) = -71\ kJ\ mol^{-1} \qquad (20b)$$

to investigate the surprising finding[36] that Mg^+ is unreactive towards N_2O, in contrast to the rapid reactions of other metallic ions such as Ca^+ [37] and Fe^+ [38] with this oxidant.

In terms of the neutral chemistry of magnesium in the MLT, Figure 1 shows that atomic Mg is oxidised rapidly by O_3 to MgO,[39] which then reacts with O_2, O_3, H_2O or CO_2.[40] A key question is: how stable is MgO_3, or other species that form from it, and do they provide a permanent sink for magnesium below 90 km? To answer this question, the reactions of MgO, MgO_2, MgO_3 and $MgCO_3$ with atomic O were studied:

$$MgO + O \rightarrow Mg + O_2 \qquad \Delta H(0\ K) = -235\ kJ\ mol^{-1} \qquad (21)$$

$$MgO_2 + O \rightarrow MgO + O_2 \qquad \Delta H(0\ K) = -172\ kJ\ mol^{-1} \qquad (22)$$

$$MgO_3 + O \rightarrow MgO_2 + O_2 \qquad \Delta H(0\ K) = -115\ kJ\ mol^{-1} \qquad (23)$$

$$MgCO_3 + O \rightarrow MgO_2 + CO_2 \qquad \Delta H(0\ K) = -117\ kJ\ mol^{-1} \qquad (24)$$

The rate coefficients of these reactions were measured using a fast flow tube with detection of Mg and MgO by laser induced fluorescence. In order to establish the technique the reaction

$$MgO + CO \rightarrow Mg + CO_2 \qquad \Delta H(0\ K) = -272\ kJ\ mol^{-1} \qquad (25)$$

was also studied, where CO can be regarded as a surrogate for atomic O.

Experimental Work

Pulsed laser photolysis/laser induced fluorescence (PLP-LIF)

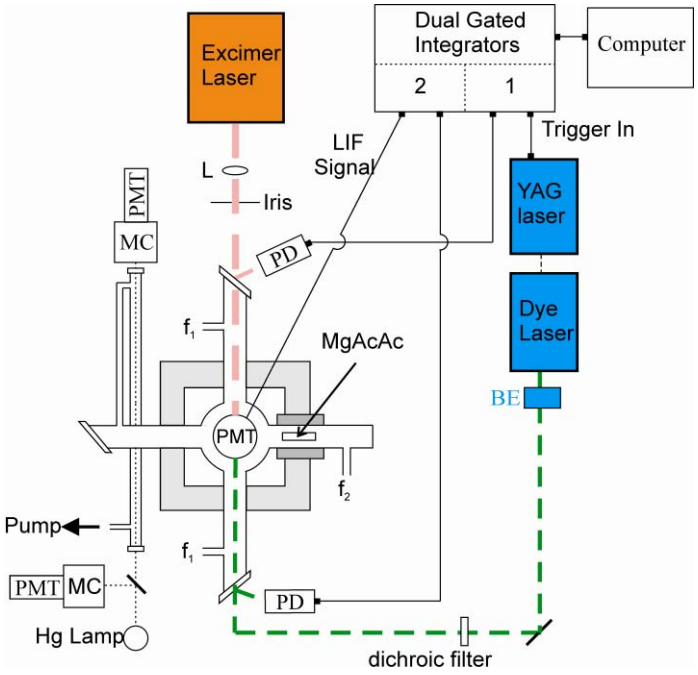

Figure 2. Schematic diagram of the pulsed laser photolysis / laser induced fluorescence apparatus: f_1, flow of reactant and He; f_2, flow of He; L = lens (f = 45cm); PMT = photomultiplier; MC= monochromator.

The pulsed laser photolysis/laser induced fluorescence (PLP-LIF) apparatus in Figure 2 has been described in detail by Plane *et al*.[41] Mg^+ was produced in the central chamber of the stainless steel reactor by pulsed multi-photon photolysis of magnesium acetyl acetonate (MgAcAc or $Mg(C_5H_7O_2)_2$) in an excess of the bath gas (He) and reactants (CO_2, H_2O, N_2, O_3 or O_2). Powdered MgAcAc was placed into a tantalum boat, located in a heat pipe connected to the central chamber, and heated to between 433 and 463 K, maintained to within ± 5 K during a particular experiment. The resulting MgAcAc vapour was entrained in the bath gas and carried to the central chamber where it then mixed with a larger flow of bath gas and reactant mixture.

The photolysis of the MgAcAc vapour at 193 nm by an ArF excimer laser (pulse energy 40-110 mJ, pulse width 25 ns, pulse rate 5 Hz) produced Mg^+ ions and initiated the reaction. The Mg^+ ions were probed at 279.6 nm ($Mg^+(3^2P\text{-}3^2S)$) using a frequency doubled Nd-YAG dye laser (Sirah, Model CBR-G-30; laser dye Rhodamine 590) frequency doubled using a BBO crystal (typical pulse energy = 400 μJ). The excimer and dye laser beams were aligned collinearly to pass through the centre of the chamber, with a dichroic mirror used to protect the dye laser from the excimer beam. The LIF signal was measured by a photomultiplier tube after passing through an interference filter centred at 280 nm (fwhm = 15 nm). The LIF signal was collected by a gated integrator, delayed for 30 ns after the dye laser pulse; the dye laser was triggered at a time delay after the excimer pulse that was scanned under computer control.

For reaction 1, the O_3 concentration was measured using UV absorption spectroscopy between 250 and 300 nm. The broad-band radiation from a deuterium lamp (Oriel, Model 60000) was passed through a 1 m pathlength absorption cell, located downstream from the central chamber, and focused into the entrance slit of a 0.5 m grating spectrometer (Spex, model 1870B) equipped with a 1200 groove mm^{-1} grating (resolution 0.12 nm FWHM). Absorption spectra were recorded with a photodiode array (EG&G, PARC 1412) and converted to optical density, before fitting reference absorption cross sections for O_3 to derive their concentrations.[42] The O_3 concentrations were corrected for wall loss and temperature difference between the reaction chamber and absorption cell.

Fast flow tube-mass spectrometer (FT-MS)

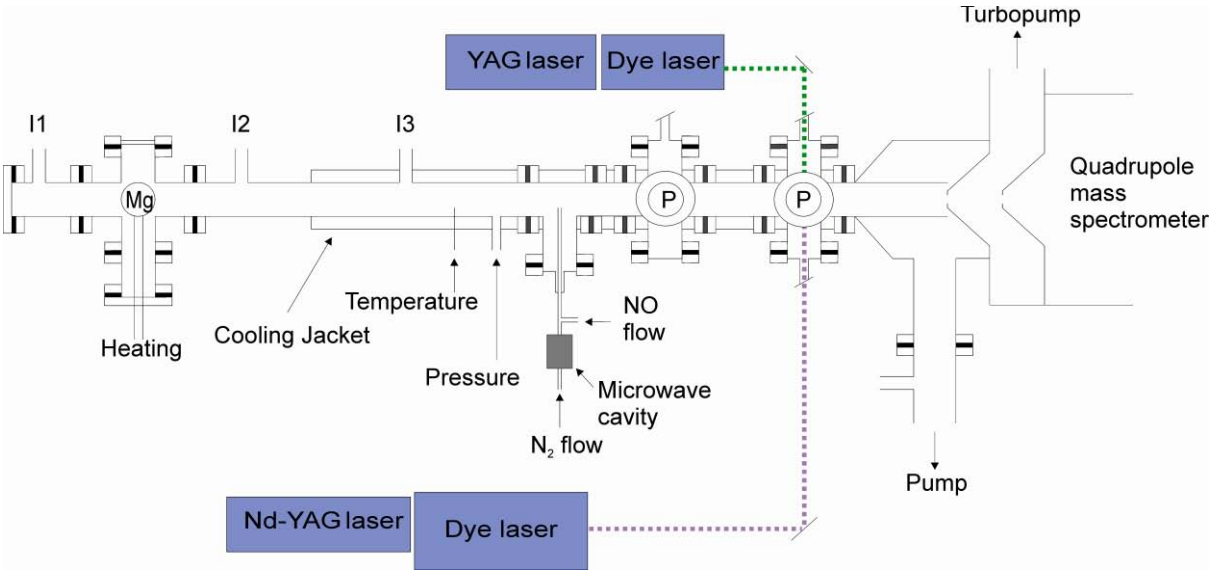

Figure 3. Schematic diagram of the fast flow tube with detection by mass spectrometry (ions) or laser induced fluorescence (neutrals).

The fast flow tube-mass spectrometer system in Figure 3 has been used previously to study both the neutral and ion-molecule reactions of Fe- and Ca-containing species.[43-46] The stainless steel flow tube (internal diameter = 37.5 mm) consists of sections of tube, cross-pieces and nipple sections connected by conflat flanges sealed with copper gaskets. The tube has a total length of 1285 mm from the carrier gas entry point to the mass spectrometer skimmer cone. Mg^+ ions were produced via laser ablation of a piece of magnesite ($MgCO_3$) using a 532 nm Nd:YAG laser (repetition rate = 10 Hz, pulse energy ~ 10mJ), loosely focused onto the target using a quartz lens (focal length = 150 mm). The ablation target was mounted on a rotary feedthrough powered by a DC motor, and projected into the centre of the cylindrical axis of the tube (not shown in

Figure 3). The target was rotated so that a fresh surface was presented to each laser pulse in order to maintain a uniform Mg^+ signal. The Mg^+ ion pulses were entrained in a flow of He which entered upstream of the ablation target. Reactants entered the flow tube via side ports downstream of the ablation target. An overall gas flow rate of 3000 sccm was used at pressures of 1.2 - 1.7 torr, creating flow velocities of 32 - 22 m s^{-1}. Hence the Reynolds number was always less that 80, ensuring laminar flow within the tube.

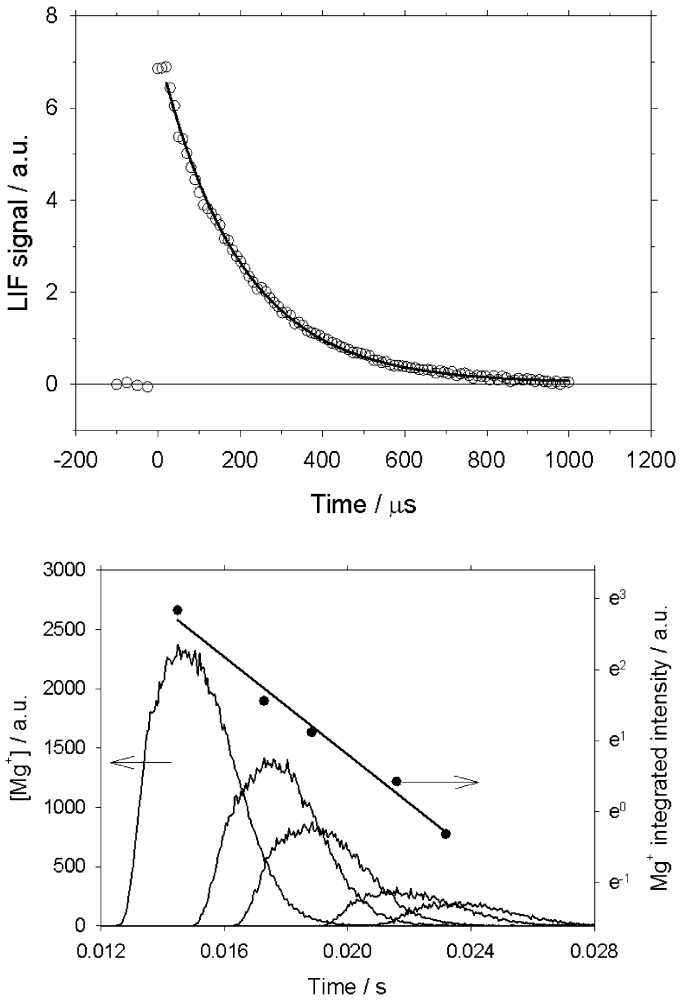

Figure 4. Top panel: time-resolved profile of the LIF signal obtained by pumping the ($Mg^+(3^2P_1)$ – Mg^+ (3^1S_0)) transition at 279.6 nm and monitoring emission at the same wavelength, following the pulsed photolysis at 193.3 nm of MgAcAc. The solid line is a fit to the form $A\ \exp^{(-k't)}$. Temperature = 190 K; Pressure = 4 Torr. Bottom panel: Diffusional loss of Mg^+ in the flow tube at 295 K. Left axis: Pulses of Mg^+ for a series of flow times at a constant pressure of 0.9 Torr. Right axis: integrated signal for these pulses (filled circles) and exponential fit yielding the diffusional loss of Mg^+.

Mg^+ and product molecular ions were detected using a differentially pumped 2-stage quadrupole mass spectrometer (VG Quadrupoles, Model SXP Elite). The entrance aperture of the skimmer cone before the first stage of the mass spectrometer was 0.1 mm diameter, located 1160 mm downstream of the ablation target. The aperture diameter of the skimmer cone before the second stage (containing the quadrupole and Channeltron electron multiplier) was 2 mm. In order to reduce the residence time of the ions between the skimmer zones, the first skimmer cone was biased by -11 to -16 V and the second by -94 V. The resulting potential difference accelerated the ions into the quadrupole and prevented the formation of clusters ions in the cold expansion after the first skimmer cone. A multi-channel scaler, synchronized with the YAG laser, was used to record the ion signal, typically from the accumulation of 10^3 laser shots.

For the neutral experiments, Mg vapour was produced by heating the metal in a crucible at about 800 K. Mg and MgO

were detected by laser induced fluorescence at 285.2 nm ($Mg(3^1P_1 - 3^1S_0)$) and 499.4 nm ($MgO(B^1\Sigma^+ - X^1\Sigma^+)$), respectively, using a pair of Nd:YAG-pumped dye lasers.

Results and Discussion

PLP-LIF measurements

The time-resolved LIF signals in the pulsed laser experiments were of a single exponential form and were well fitted by the form $A.\exp(-k't)$, as shown in Figure 4 (top panel). The loss of Mg^+ is described by the pseudo first-order decay coefficient k', since the concentrations of the reactant and bath gas were kept well in excess of Mg^+. For reaction with O_3 (reaction 1),

$$k' = k_{DiffMg^+} + k_{MgAcAc}[MgAcAc] + k_1[O_3] \qquad (I)$$

where k_{DiffMg^+} describes the diffusion of the Mg^+ ions out of the volume defined by the intersection of the laser beams within the field of view of the photomultiplier tube, and k_{MgAcAc} is the rate coefficient for the reaction between Mg^+ and the organometallic precursor. The value of (k_{DiffMg^+} + k_{MgX}[MgAcAc]) was determined from a fit of the LIF decay when $[O_3] = 0$, and ranged from 3000 – 20000 s^{-1} depending on the heat-pipe temperature for a particular experiment. Plots of k' versus $[O_3]$, which should be linear, showed marked curvature at large $[O_3]$. This behaviour is caused by reaction 16a recycling MgO^+ back to Mg^+. This problem was overcome by adding HCl, which removes MgO^+ via reaction 21:

$$MgO^+ + HCl \rightarrow MgCl^+ + OH \qquad \Delta H(0\ K) = -83\ kJ\ mol^{-1} \qquad (26a)$$

$$\rightarrow MgOH^+ + Cl \qquad \Delta H(0\ K) = -91\ kJ\ mol^{-1} \qquad (26b)$$

The rate coefficient k_{16} for the reaction between MgO^+ and O_3, and the branching ratio f_{16a} to form Mg^+ (i.e., k_{16a}/k_{16}), were then estimated by modelling the observed dependence of k' on $[O_3]$ in the absence of HCl.

For the recombination reactions between Mg^+ and X in the presence of He

$$k' = k_{DiffMg^+} + k_{MgAcAc}[MgAcAc] + k_X[X][He] \qquad (II)$$

the rate was measured both as a function of [X] and [He]. Reaction 4 was also studied at high CO_2 concentrations to obtain the relative efficiency of CO_2 compared to He as third body.

FT-MS measurements

Figure 1 (bottom panel) illustrates a sequence of time-resolved Mg^+ pulses measured by the mass spectrometer at the downstream end of the flow tube. For kinetic measurements, the relative ion concentration can be determined either from the pulse height or the integrated area of each pulse, which gives essentially the same result. As an example, the first-order removal rate of Mg^+ in reaction 3 was obtained from the relation:[46]

$$k' = k_3[O_2][He] = -\frac{\ln\left(\frac{[Mg^+]^t_{O_2}}{[Mg^+]^t_0}\right)}{t} \qquad \text{(III)}$$

where t is the time between the injection point of O_2 into the flow tube and the downstream skimmer cone; $[Mg^+]^t_{O_2}$ and $[Mg^+]^t_0$ are the measured ion signals in the presence and absence of O_2, respectively. t is calculated from the measured velocity of the Mg^+ pulse travelling down the tube, and is then reduced by 5% to correct for the O_2 mixing by diffusion from the injection point at the wall across the centre of the flow tube. Radial diffusion and loss on the flow tube walls is significant in the FT-MS system. This was therefore measured for each species – ions, atomic O – and included in a model of the flow tube kinetics.

The addition of a second ligand X to $Mg^+.X$ was studied by monitoring the dependence of $Mg^+.X$ on [X], which is described by the following differential equations:

$$\frac{d[Mg^+]}{dt} = -k_{diff,Mg^+}[Mg^+] - k_X[Mg^+][X] \qquad \text{(IV)}$$

$$\frac{d[Mg^+.X]}{dt} = -k_{diff,Mg^+.X}[Mg^+.X] + k_X[Mg^+][X] - k_{X2}[Mg^+.X][X] \qquad \text{(V)}$$

where k_X is the second-order rate coefficient for the reaction between Mg^+ and X, k_{X2} is the second-order rate coefficient for the reaction between $Mg^+.X$ and X, and k_{diff} is the rate of wall loss by diffusion and uptake. Equations IV and V were solved numerically using 4th-order Runge-Kutta integration to find the value of k_{X2} which best fitted the experimental data points (using a χ^2 minimisation[46]). The statistical uncertainty in k_{X2} was estimated from the standard deviation of the difference between k_{X2} obtained from a fit to each individual experimental point, and the value from the global fit. The overall systematic error was then estimated by using a Monte Carlo procedure which varied the model parameters within their 1σ uncertainty range (10^4 times) and repeating a global fit to the experimental points. The ligand-exchange reactions ($Mg^+.X + Y \rightarrow Mg^+.Y + X$) and the neutral reactions were studied in a similar way.

The results of all the ion-molecule work are summarised in Table 1, and the neutral reactions are listed in Table 2.

Table 1. Measured rate coefficients for ion-molecule reactions (1σ uncertainties).

	Reaction	k(295 K unless specified) cm^3 $molecule^{-1}$ s^{-1}
1	$Mg^+ + O_3 \rightarrow MgO^+ + O_2$	$(1.2 \pm 0.2) \times 10^{-9}$ (190 - 340 K)
2	$Mg^+ + N_2 + (He) \rightarrow Mg^+.N_2$	$(2.7 \pm 0.3) \times 10^{-31}$ $(T/300\ K)^{-1.88}$ [a] (190 K)
3	$Mg^+ + O_2 (+ He) \rightarrow MgO_2^+$	$(3.5 \pm 0.3) \times 10^{-31}$ $(T/300\ K)^{(-2.55 \pm 0.14)}$ [a] (190–299 K)
4	$Mg^+ + CO_2 (+ He) \rightarrow Mg^+.CO_2$	$(7.1 \pm 1.1) \times 10^{-30}$ $(T/300\ K)^{(-1.86 \pm 0.03)}$ [a] (190–403 K)
4a	$Mg^+ + CO_2 (+ CO_2) \rightarrow Mg^+.CO_2$	(5.3 ± 0.7) x 10^{-29} $(T/300\ K)^{(-1.86 \pm 0.03)}$ [a] (190 – 403 K)
5	$Mg^+ + H_2O \rightarrow Mg^+.H_2O + He$	$(2.7 \pm 0.3) \times 10^{-29}$ $(T/300\ K)^{-2.58}$ [a]
6	$Mg^+.CO_2 + H_2O \rightarrow Mg^+.H_2O + CO_2$	$(5.1 \pm 0.9) \times 10^{-11}$
7	$MgO_2^+ + H_2O \rightarrow Mg^+.H_2O + O_2$	$(1.9 \pm 0.6) \times 10^{-11}$
8	$Mg^+.CO_2 + O_2 \rightarrow Mg^+.O_2 + CO_2$	$(2.2 \pm 0.8) \times 10^{-11}$
9	$Mg^+.N_2 + O_2 \rightarrow Mg^+.O_2 + N_2$	$(3.5 \pm 1.5) \times 10^{-12}$
10	$MgO_2^+ + O_2 \rightarrow MgO_2^+.O_2$	$(3.3 \pm 0.3) \times 10^{-13}$ [b]
11	$Mg^+.CO_2 + CO_2 \rightarrow Mg^+.(CO_2)_2$	$(8.9 \pm 3.8) \times 10^{-13}$ [b]
12	$Mg^+.H_2O + H_2O \rightarrow Mg^+.(H_2O)_2$	$(2.6 \pm 0.4) \times 10^{-12}$ [b]
13	$MgO_2^+ + N_2 \rightarrow MgO_2^+.N_2$	$(1.9 \pm 0.4) \times 10^{-13}$ [b]
14	$MgO_2^+ + CO_2 \rightarrow MgO_2^+.CO_2$	$(7.4 \pm 1.2) \times 10^{-12}$ [b]
15	$Mg^+.H_2O + O_2 \rightarrow MgO_2^+.H_2O$	$(1.5 \pm 0.5) \times 10^{-11}$ [b]
16	$MgO^+ + O_3 \rightarrow Mg^+ + 2O_2$	$(3.0 \pm 1.5) \times 10^{-10}$
	$\rightarrow MgO_2^+ + O_2$	$(5.5 \pm 1.5) \times 10^{-10}$
17	$MgO_2^+ + O \rightarrow MgO^+ + O_2$	$(6.5 \pm 1.8) \times 10^{-10}$

18	$MgO^+ + O \rightarrow Mg^+ + O_2$	$(5.9 \pm 2.4) \times 10^{-10}$
19	$Mg^+ + N_2O \rightarrow MgO^+ + N_2$	$(5.8 \pm 1.4) \times 10^{-30}$ (T/300 K)$^{(-1.94 \pm 0.08)}$ [a] (193 – 373 K)

[a] Units: cm^6 $molecule^{-2}$ s^{-1}. [b] Association reaction at a pressure of 1.2 Torr

Table 2. Measured rate coefficients for reactions of neutral Mg species (1σ uncertainties).

	Reaction	*k*(295 K) cm^3 $molecule^{-1}$ s^{-1}
21	$MgO + O \rightarrow Mg + O_2$	$(6.2 \pm 1.1) \times 10^{-10}$
22	$MgO_2 + O \rightarrow MgO + O_2$	$(8.4 \pm 2.8) \times 10^{-11}$
23	$MgO_3 + O \rightarrow MgO_2 + O_2$	$< 5 \times 10^{-13}$ [a]
24	$MgCO_3 + O \rightarrow MgO_2 + CO_2$	$(6.7 \pm 1.8) \times 10^{-12}$
25	$MgO + CO \rightarrow Mg + CO_2$	$(1.1 \pm 0.9) \times 10^{-11}$

[a] This measurement is complicated by the probable recombination of MgO_2 with O_2 to form MgO_4, so the upper limit describes the overall reduction of MgO_3 to Mg.

Theoretical calculations

In collaboration with Prof. Timothy Wright (University of Nottingham) we carried out a set of high-level quantum theory calculations on the $Mg^+.X$ and $X.Mg^+.Y$ clusters. B3LYP optimizations were performed employing 6-311+G(2d,p) basis sets. In several cases a number of different orientations were investigated in order to determine the geometries of lowest energy; and in cases involving O and O_2, different spin states were also considered. In order to establish accurate dissociation energeties, up to RCCSD(T) single-point energy calculations were also employed, using quadruple-ζ basis sets.[29] Figure 5 illustrates the optimised geometries of some of these clusters. These calculations provided the input data - vibrational frequencies, rotational constants and energetics - required for Rice-Ramsperger-Kassell-Markus (RRKM) theory calculations which enabling rate coefficients to be extrapolated to temperatures and pressures that are not achievable in the laboratory. Figure 6 illustrates RRKM fits to the measured rate

coefficients for the ion-molecule association reactions. This shows that some of these reactions (e.g. $Mg^+ + H_2O$) are significantly in the "fall-off" region between third- and second-order kinetic behaviour even at a pressure of 12 Torr.

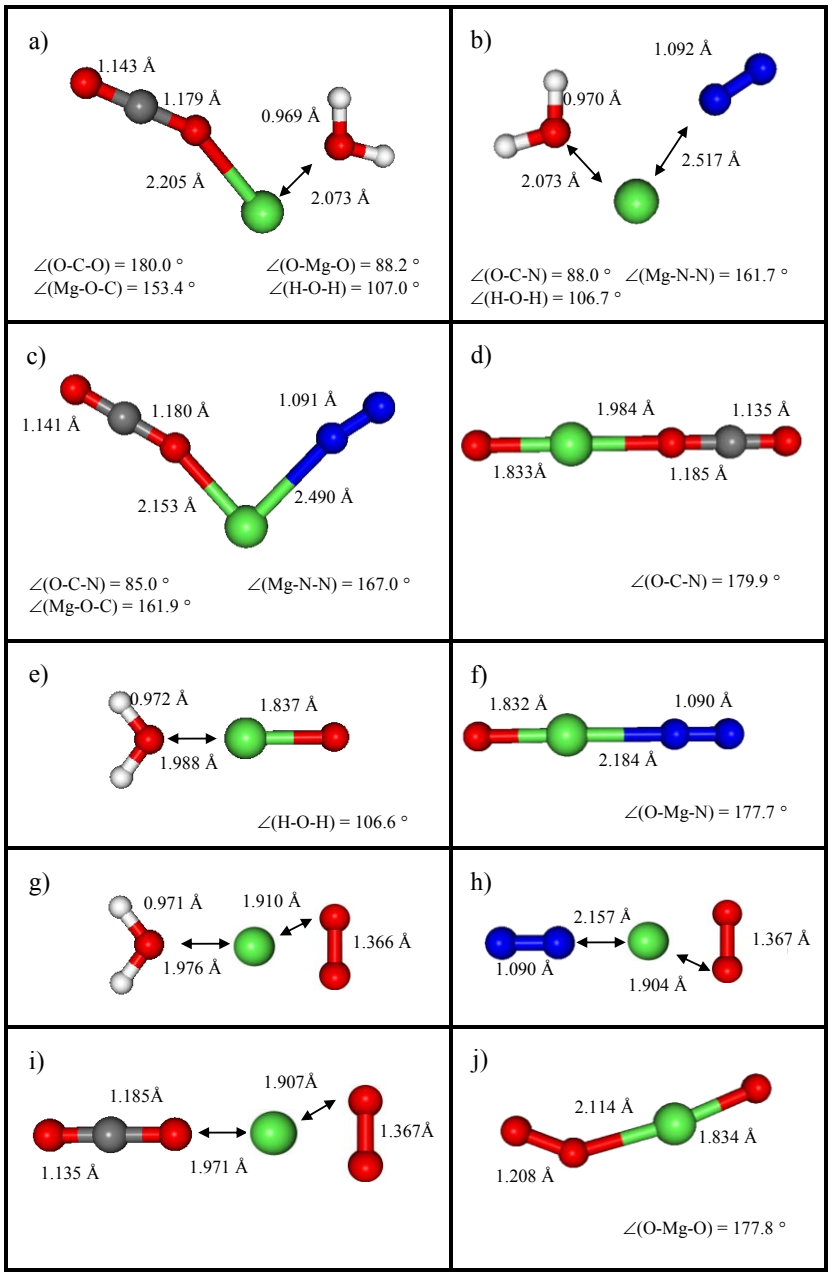

Figure 5. Geometries of $[X\text{-}Mg\text{-}Y]^+$ complexes, optimized using the B3LYP/6-311+g(2d,p) level of quantum theory. Mg = green; N = blue; O = red; C = black; H = white.

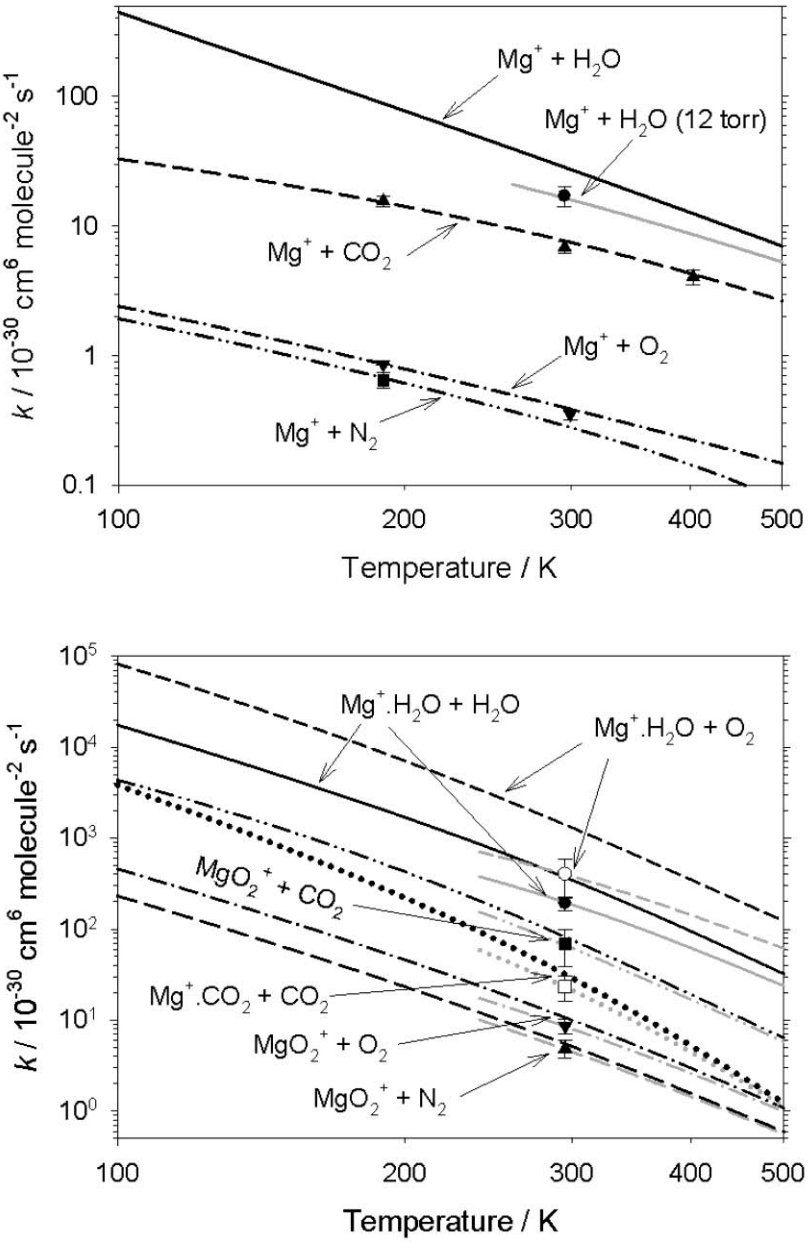

Figure 6. Top panel: third-order rate coefficients for the recombination of Mg^+ with H_2O, CO_2, O_2 and N_2 as a function of temperature, with M = He. The black lines are low pressure limiting rate coefficients obtained from fits of RRKM theory to the experimental data. The discrete symbols are the experimental data taken at 12 Torr. This shows that the measured rate coefficients for CO_2, O_2 and N_2 are essentially at their low pressure limits, whereas the H_2O rate coefficient shows significant fall-off, illustrated by the RRKM fit at 12 Torr (grey solid line). Bottom panel: third-order rate coefficients for the recombination of $Mg^+.H_2O$, $Mg^+.CO_2$ and MgO_2^+ ions with H_2O, CO_2, O_2 and/or N_2 as a function of temperature, with M = He. The discrete points are experimental measurements at a pressure of 1.2 Torr. The grey lines show RRKM fits at this pressure, and the black lines indicate the low pressure limiting rate coefficients.

Satellite retrievals

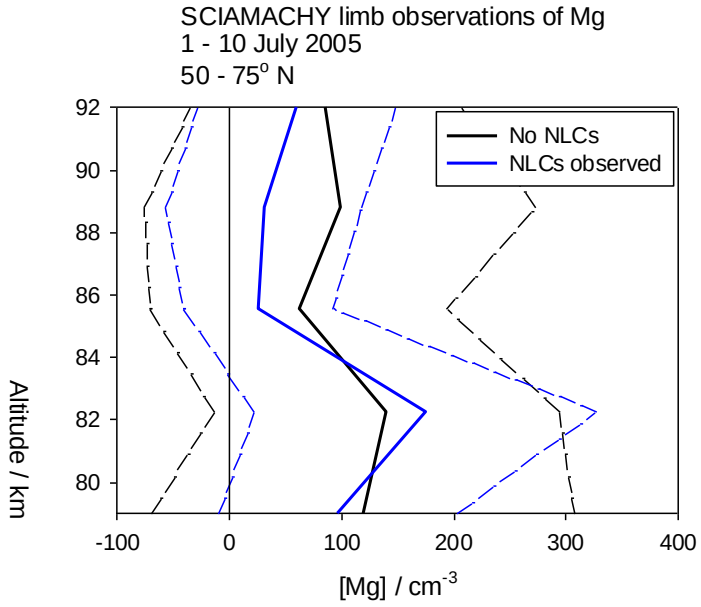

Figure 7. Retrieved average vertical profiles of atomic Mg in the presence and absence of noctilucent clouds (NLCs).The broken lines indicate 2σ uncertainties.

Charlotte Whalley and the PI travelled to the University of Bremen in May 2009 to work with Dr Miriam Sinnhuber on SCIAMACHY retrievals of Mg and Mg^+. An important result of this work is that atomic Mg *does not disappear in the presence of noctilucent clouds*. These ice clouds form in the summer at high latitudes, at an altitude of about 83 km. All other meteoric metals - Na, Fe, K - are rapidly removed in the presence of the clouds,[47-49] so that there are insignificant concentations of these metal atoms below 85 km. However, as shown in Figure 7, there is no significant difference in the profile of atomic Mg retrieved from SCIAMACHY when ice clouds are present. We have shown using quantum calculations that the reason for this unexpected result is that Mg atoms stick much less strongly to an ice surface - the binding energy is only 20 kJ mol^{-1}, compared to more than 30 kJ mol^{-1} for these other metals, so that a Mg atom will desorb in less than 1 ms even at 130 K.

Atmospheric Modelling

Mars

Low-lying plasma layers have been observed sporadically in the Martian atmosphere by radio occultation measurements from spacecraft such as the Mars Express Orbiter[50] and the Mars Global Surveyor. [51] These layers are just a few km wide, and tend to occur around 90 km. It has been proposed that the layers consist of metallic ions, for two reasons: they occur in the aerobraking region of the planet where meteoroids ablate; and they resemble sporadic *E* layers in the terrestrial atmosphere which are known to be composed principally of Fe^+ and Mg^+ ions. The rate coefficients measured in the EOARD project were used to solve the problem of how metallic

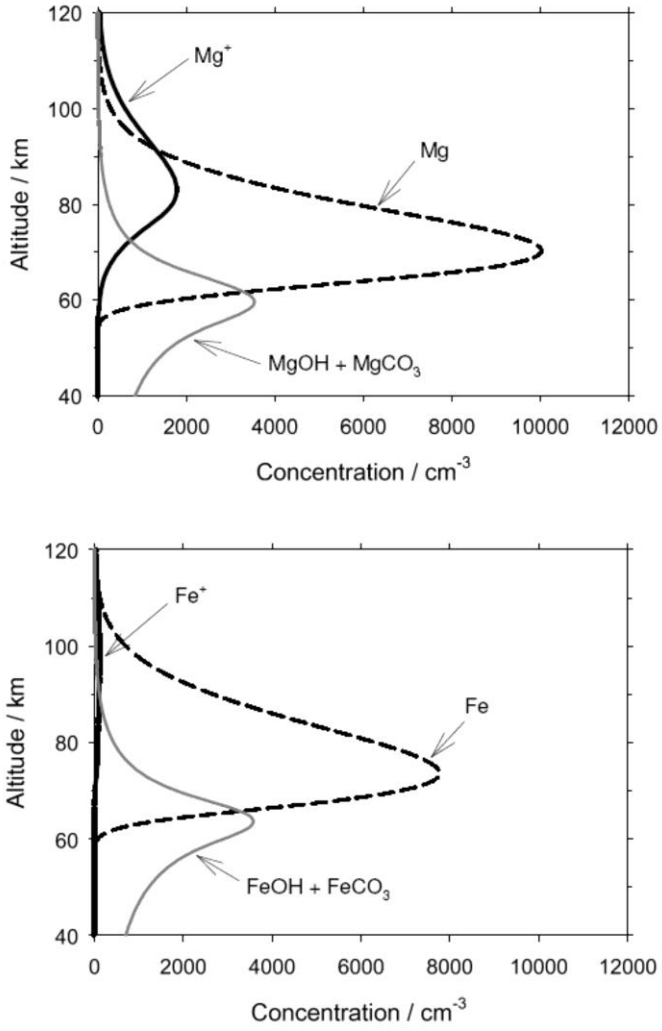

Figure 8. Top panel: modelled height profiles of Mg^+, Mg and the neutral magnesium reservoirs, for the globally-averaged Martian atmosphere during daytime. Bottom panel: height profiles of the corresponding iron species. Note the almost complete absence of Fe^+, because the reactions of FeO_2^+ and FeO^+ with atomic O are about 20 times slower than the analogous reactions of MgO_2^+ and MgO^+ (reactions 17 and 18).

ions can persist in a CO_2-rich atmosphere, where the ions should be neutralized rapidly by formation of metal-CO_2 cluster ions followed by dissociative electron recombination.[32]

A model of magnesium and iron chemistry in the Martian atmosphere was constructed, which includes meteoric differential ablation rates calculated with the Leeds CABMOD model,[2] photo-ionization, and gas-phase ion-molecule and neutral chemistry. As shown in Figure 8, the model predicts that nearly all the metallic ions between 70 and 110 km should be Mg^+, because the reactions of MgO_2^+ and MgO^+ with atomic O (reactions 17 and 18) are fast enough to prevent these molecular ions undergoing dissociative electron recombination (unlike the analogous Fe species). There are enough Mg^+ ions to form sporadic layers of the observed plasma density, and the layers can have a lifetime against neutralization in excess of 20 hours.

Earth

Above 85 km in the terrestrial atmosphere, reaction 1 ($Mg^+ + O_3$) is the dominant removal process of Mg^+, although the resulting MgO^+ is mostly recycled back to Mg^+ by reaction 18 ($MgO^+ + O$). Below 85 km, reaction 2 ($Mg^+ + N_2$) becomes more rapid, followed by reaction 3 ($Mg^+ + O_2$). However, the resulting $Mg^+.N_2$ will switch with O_2 (reaction 9), so that MgO_2^+ is

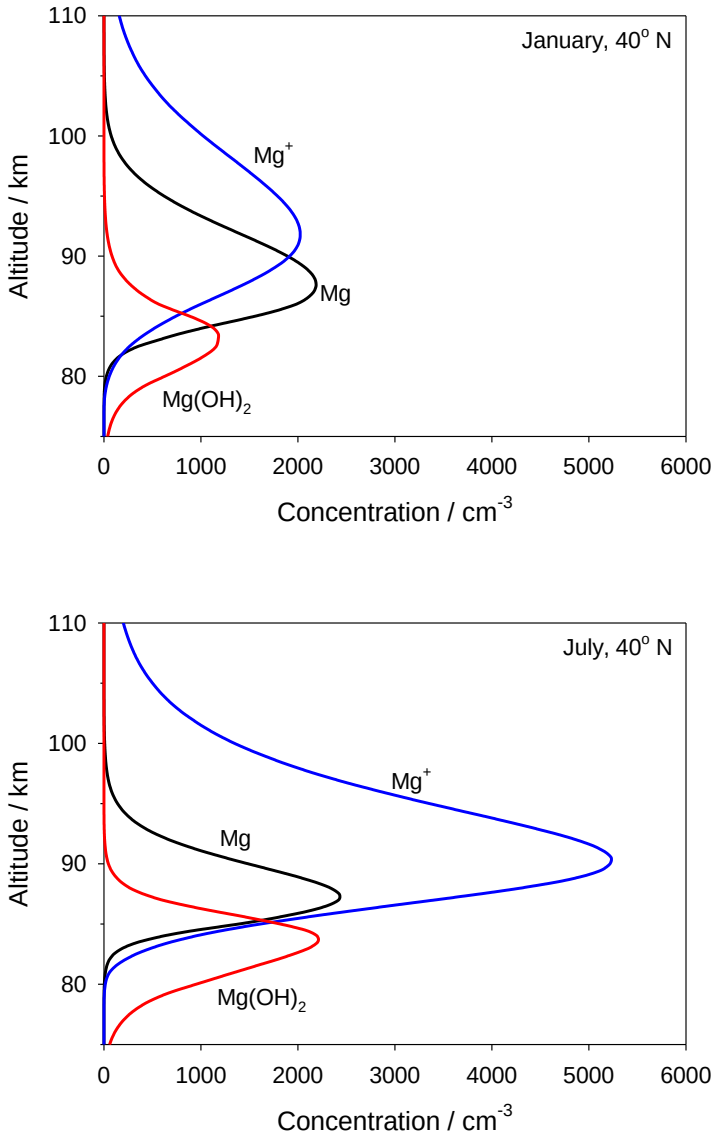

Figure 9. Vertical profiles of Mg^+, Mg and $Mg(OH)_2$ predicted by a 1-D atmospheric model for January and July, at mid-latitudes (40°N).

predicted to be the major molecular ion below 85 km. Eventually MgO_2^+ will switch with H_2O (reaction 7), react with atomic O (reaction 17), or undergo DR with an electron.

This chemistry has a dramatic effect on the lifetime of Mg^+ in an E_s layer. The electron concentration of an E_s layer is related to the critical frequency (fE_s) required for radio transmission through the layer. Mg^+ in a strong layer (fE_s = 6 MHz, $[e^-] = 5 \times 10^5$ cm^{-3}) should have a lifetime of ~ 1 hour at 90 km, but only 6 minutes at 85 km. In contrast, the Mg^+ in a weak layer ($fE_s < 2$ MHz, $[e^-] < 5 \times 10^4$ cm^{-3}), should have a lifetime of about 10 hours at 90 km. In fact, comparison with our previous work on the lifetimes of Fe^+ [44] and Ca^+ [46] in sporadic E layers shows that Mg^+ has a much longer lifetime below 95 km. This arises because $k_{18}(MgO^+ + O \rightarrow Mg^+ + O_2)$ is about 20 times faster than the analogous reactions of FeO^+ [44] and CaO^+.[46] The longer lifetime of Mg^+ (by roughly an order of magnitude) below 90 km is consistent with recent limb-scanning satellite measurements of Mg^+, which show significant concentrations of this ion below this altitude.[17]

The rate coefficients measured in this EOARD project (Table 1), together with our previous work on Mg and MgO reactions,[39,40] were then inserted into a time-resolved 1-D model between 65 and 110 km region, with 0.5 km resolution. The new model, MagMOD, is similar in structure to one developed for sodium chemistry in the MLT, including the source s of the minor constituents (O_3, O, NO^+ etc.) which control the magnesium chemistry.[52] The only tuneable

parameter in the model is the meteoric ablation flux of Mg. The annual average flux was set to 8200 Mg atom cm^{-2} s^{-1}, and this was then varied seasonally according to the radio meteor rate.[53] Figure 9 illustrates the model predictions of Mg^+, Mg and $Mg(OH)_2$ in the MLT, for January and July at mid-latitudes. This shows a 3-fold increase in the Mg^+ column abundance, from 3.0×10^9 in winter to 6.1×10^9 cm^{-2} in summer. This is in very good agreement with the GOME[16] and SCIAMACHY[18] satellite measurements. The peak height of the Mg^+ layer is between 90 and 100 km, with peak densities between 2000 and 5000 cm^{-3}, in accord with rocket-borne mass spectrometric measurements.[22,25]

The neutral Mg layer, in contrast, is predicted to exhibit little seasonal variation, with a small decrease from 2.1×10^9 cm^{-2} in January to 1.5×10^9 cm^{-2} in July. This agrees well with the satellite record[16,18] The predicted peak of the Mg layer around 88 km is in accord with Mg profiles retrieved from SCIAMACHY limb-scanning measurements.[17]

In 2011, MagMOD will be incorporated into the *Whole Atmosphere Chemistry Climate Model (WACCM)*, produced by the National Center for Atmospheric Research (Boulder). This general circulation model, which extends from the surface to 140 km, will then be used to explore the global variation of Mg and Mg^+.

References

1. Hughes, D. W., in *Cosmic Dust*, ed. M. J.A.M., Wiley, London, 1978.
2. Vondrak, T., J. M. C. Plane, S. Broadley and D. Janches, *Atmos. Chem. Phys.*, 2008, **8**, 7015-7031.
3. Anderson, J. G. and C. A. Barth, *Journal of Geophysical Research*, 1971, **76**, 3723-&.
4. Steinweg, A., D. Krankowsky, P. Lammerzahl and B. Anweiler, *Journal of Atmospheric and Terrestrial Physics*, 1992, **54**, 703-714.
5. Aikin, A. C., J. M. Grebowsky and J. P. Burrows, in *Impact of Minor Bodies of Our Solar System on Planets and Their Middle and Upper Atmosphere*, 2004, vol. 33, pp. 1481-1485.
6. Fesen, C. G. and P. B. Hays, *Journal of Geophysical Research-Space Physics*, 1982, **87**, 9217-9223.
7. Gardner, J. A., R. A. Viereck, E. Murad, D. J. Knecht, C. P. Pike, A. L. Broadfoot and E. R. Anderson, *Geophysical Research Letters*, 1995, **22**, 2119-2122.
8. Gardner, J. A., A. L. Broadfoot, W. J. McNeil, S. T. Lai and E. Murad, *Journal of Atmospheric and Solar-Terrestrial Physics*, 1999, **61**, 545-562.
9. Gerard, J. C. and A. Monfils, *Journal of Geophysical Research-Space Physics*, 1978, **83**, 4389-4391.
10. Joiner, J. and A. C. Aikin, *Journal of Geophysical Research-Space Physics*, 1996, **101**, 5239-5249.
11. Mende, S. B., G. R. Swenson and K. L. Miller, *Journal of Geophysical Research-Space Physics*, 1985, **90**, 6667-6673.
12. Minschwaner, K., D. Herceg, S. A. Budzien, K. F. Dymond, C. Fortna and R. P. McCoy, *Journal of Geophysical Research-Space Physics*, 2007, **112**.
13. Scharringhausen, M., A. C. Aikin, J. P. Burrows and M. Sinnhuber, *Atmospheric Chemistry and Physics*, 2008, **8**, 1963-1983.
14. Scharringhausen, M., A. C. Aikin, J. P. Burrows and M. Sinnhuber, *Journal of Geophysical Research-Atmospheres*, 2008, **113**.
15. Correira, J., A. C. Aikin, J. M. Grebowsky, W. D. Pesnell and J. P. Burrows, *Geophysical Research Letters*, 2008, **35**, 6.

16. Correira, J., A. C. Aikin, J. M. Grebowsky, W. D. Pesnell and J. P. Burrows, *Geophys. Res. Lett.*, 2008, **35**, art. no.: L06103.
17. Scharringhausen, M., A. C. Aikin, J. P. Burrows and M. Sinnhuber, *Atmos. Chem. Phys.*, 2008, **8**, 1963-1983.
18. Scharringhausen, M., A. C. Aikin, J. P. Burrows and M. Sinnhuber, *J. Geophys. Res.*, 2008, **113**, art. no.: D13303.
19. Swider, W., *Planetary and Space Science*, 1984, **32**, 307-312.
20. Scharringhausen, M., University of Bremen, 2007.
21. Helmer, M., J. M. C. Plane, J. Qian and C. S. Gardner, *Journal of Geophysical Research-Atmospheres*, 1998, **103**, 10913-10925.
22. Grebowsky, J. M. and A. C. Aikin, in *Meteors in the Earth's Atmosphere*, ed. E. Murad and I. P. Williams, Cambridge University Press, Cambridge, 2002.
23. Kopp, E., *Journal of Geophysical Research-Space Physics*, 1997, **102**, 9667-9674.
24. Gerding, M., M. Alpers, U. von Zahn, R. J. Rollason and J. M. C. Plane, *Journal of Geophysical Research-Space Physics*, 2000, **105**, 27131-27146.
25. Kopp, E., *J. Geophys. Res.*, 1997, **102**, 9667-9674.
26. Mathews, J. D., *J. Atmos. Solar-Terr. Phys.*, 1998, **60**, 413-435.
27. Plane, J. M. C., *Chem. Rev.*, 2003, **103**, 4963-4984.
28. Plane, J. M. C. and M. Helmer, *Faraday Discussions*, 1995, 411-430.
29. Plowright, R. J., T. J. McDonnell, T. G. Wright and J. M. C. Plane, *J. Phys. Chem. A*, 2009, **113**, 9354-9364.
30. Ferguson, E. E. and F. C. Fehsenfeld, *J. Geophys. Res.*, 1968, **73**, 6215-&.
31. Rowe, B. R., D. W. Fahey, E. E. Ferguson and F. C. Fehsenfeld, *J. Chem. Phys.*, 1981, **75**, 3325-3328.
32. Whalley, C. L. and J. M. C. Plane, *Faraday Disc.*, 2010, **147**, 349-368.
33. Robbins, D. L., L. R. Brock, J. S. Pilgrim and M. A. Duncan, *J. Chem. Phys.*, 1995, **102**, 1481-1492.
34. Martinez-Nunez, E., C. L. Whalley, D. Shalashilin and J. M. C. Plane, *J. Phys. Chem. A*, 2010, **114**, 6472-6479.
35. Bjorn, L. G., E. Kopp, U. Herrmann, P. Eberhardt, P. H. G. Dickinson, D. J. Mackinnon, F. Arnold, G. Witt, A. Lundin and D. B. Jenkins, *J. Geophys. Res.*, 1985, **90**, 7985-7998.
36. Milburn, R. K., V. Baranov, A. C. Hopkinson and D. K. Bohme, *J. Phys. Chem. A*, 1999, **103**, 6373-6382.
37. Plane, J. M. C., T. Vondrak, S. Broadley, B. Cosic, A. Ermoline and A. Fontijn, *J. Phys. Chem. A*, 2006, **110**, 7874-7881.
38. Plane, J. M. C. and R. J. Rollason, *J. Chem. Soc. Faraday Trans. 2*, 1996, **92**, 4371-4376.
39. Plane, J. M. C. and M. Helmer, *Faraday Disc.*, 1995, 411-430.
40. Rollason, R. J. and J. M. C. Plane, *Phys. Chem. Chem. Phys.*, 2001, **3**, 4733-4740.
41. Plane, J. M. C., T. Vondrak, S. Broadley, B. Cosic, A. Ermoline and A. Fontijn, *Journal of Physical Chemistry A*, 2006, **110**, 7874-7881.
42. Burrows, J. P., A. Richter, A. Dehn, B. Deters, S. Himmelmann and J. Orphal, *J. Quant. Spectrosc. Radiat. Transf.*, 1999, **61**, 509-517.
43. Vondrak, T., K. R. I. Woodcock and J. M. C. Plane, *Phys. Chem. Chem. Phys.*, 2006, **8**, 503-512.
44. Woodcock, K. R. S., T. Vondrak, S. R. Meech and J. M. C. Plane, *Phys. Chem. Chem. Phys.*, 2006, **8**, 1812-1821.
45. Broadley, S. L., T. Vondrak and J. M. C. Plane, *Phys. Chem. Chem. Phys.*, 2007, **9**, 4357-4369.
46. Broadley, S., T. Vondrak, T. G. Wright and J. M. C. Plane, *Phys. Chem. Chem. Phys.*, 2008, **10**, 5287-5298.
47. Plane, J. M. C., B. J. Murray, X. Z. Chu and C. S. Gardner, *Science*, 2004, **304**, 426-428.
48. Gardner, C. S., J. M. C. Plane, W. L. Pan, T. Vondrak, B. J. Murray and X. Z. Chu, *Journal of Geophysical Research-Atmospheres*, 2005, **110**, Article Number: D10302
49. Raizada, S., M. Rapp, F. J. Lubken, J. Hoffner, M. Zecha and J. M. C. Plane, *Journal of Geophysical Research-Atmospheres*, 2007, **112**, Article Number: D08307.
50. Pätzold, M., S. Tellman, B. Häusler, D. Hinson, R. Schaa and G. L. Tyler, *Science*, 2005, **310**, 837-839.
51. Withers, P., M. Mendillo, D. P. Hinson and K. Cahoy, *J. Geophys. Res.*, 2008, **113**, Article Number: A12314.
52. Plane, J. M. C., *Atmos. Chem. Phys.*, 2004, **4**, 627-638.
53. Yrjola, I. and P. Jenniskens, *Astron. Astrophys.*, 1998, **330**, 739-752.